



First observation and measurement of the branching fraction for the decay $B_s^0 \rightarrow D_s^{*\mp} K^\pm$

The LHCb collaboration[†]

Abstract

The first observation of the $B_s^0 \rightarrow D_s^{*\mp} K^\pm$ decay is reported using 3.0 fb^{-1} of proton-proton collision data collected by the LHCb experiment. The $D_s^{*\mp}$ mesons are reconstructed through the decay chain $D_s^{*\mp} \rightarrow \gamma D_s^\mp (K^\mp K^\pm \pi^\mp)$. The branching fraction relative to that for $B_s^0 \rightarrow D_s^{*-} \pi^+$ decays is measured to be

$$\mathcal{B}(B_s^0 \rightarrow D_s^{*\mp} K^\pm) / \mathcal{B}(B_s^0 \rightarrow D_s^{*-} \pi^+) = 0.068 \pm 0.005_{-0.002}^{+0.003},$$

where the first uncertainty is statistical and the second is systematic. Using a recent measurement of $\mathcal{B}(B_s^0 \rightarrow D_s^{*-} \pi^+)$, the absolute branching fraction of $B_s^0 \rightarrow D_s^{*\mp} K^\pm$ is measured as

$$\mathcal{B}(B_s^0 \rightarrow D_s^{*\mp} K^\pm) = (16.3 \pm 1.2 \text{ (stat)} \text{ }_{-0.5}^{+0.7} \text{ (syst)} \pm 4.8 \text{ (norm)}) \times 10^{-5},$$

where the third uncertainty is due to the uncertainty on the branching fraction of the normalisation channel.

Submitted to JHEP

© CERN on behalf of the LHCb collaboration, license CC-BY-4.0.

[†]Authors are listed at the end of this paper.

1 Introduction

The weak phase γ is one of the least well-determined CKM parameters. It can be measured using time-independent decay¹ rates, such as those of $B^+ \rightarrow \bar{D}^0 K^+$ or by time-dependent studies of $B_s^0 \rightarrow D_s^{(*)\mp} K^\pm$ decays [1]. In time-dependent measurements with the decays $B_{(s)}^0 \rightarrow D_{(s)}^{(*)-} h^+$, where h indicates a light meson, the sensitivity to γ is a consequence of the interference between the amplitudes of the $b \rightarrow u$ and $b \rightarrow c$ transitions occurring through $B_{(s)}^0$ - $\bar{B}_{(s)}^0$ mixing. The relevant Feynman diagrams for the B_s^0 system are shown in Fig. 1.

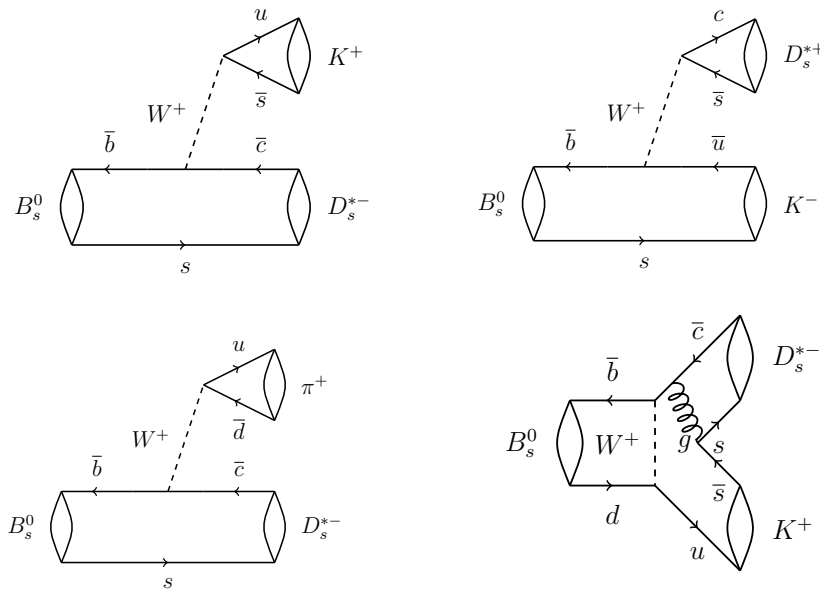


Figure 1: Feynman diagrams of the processes under study. The upper diagrams represent the two tree topologies ($b \rightarrow c$ and $b \rightarrow u$ transitions, respectively) by which a B_s^0 meson decays into the $D_s^{*\mp} K^\pm$ final state; the lower diagrams show the tree diagram of $B_s^0 \rightarrow D_s^{*-} \pi^+$ and the W -exchange topology of $B_s^0 \rightarrow D_s^{*-} K^+$.

The $B_s^0 \rightarrow D_s^\mp K^\pm$ decay mode has already been used by LHCb to determine γ with a statistical precision of about 30° [2], in an analysis based on data corresponding to an integrated luminosity of 1 fb^{-1} . An attractive feature of $B_s^0 \rightarrow D_s^{*\mp} K^\pm$ decays is that the theoretical formalism that relates the measured CP asymmetries to γ is the same as for $B_s^0 \rightarrow D_s^\mp K^\pm$ decays, when the angular momentum of the final state is taken into account in the time evolution of the B_s^0 - \bar{B}_s^0 decay asymmetries.

The observables of the decay $B_s^0 \rightarrow D_s^{(*)\mp} K^\pm$ can be related to those of $B^0 \rightarrow D^{(*)-} \pi^+$ as described in Ref. [1] through the U -spin symmetry of strong interactions. This opens the possibility of a combined extraction of γ . In addition, there is a higher sensitivity to

¹Charge-conjugate states are implied throughout.

γ in $B_s^0 \rightarrow D_s^{(*)\mp} K^\pm$ decays than in $B^0 \rightarrow D^{(*)-} \pi^+$ decays due to the larger interference between the $b \rightarrow u$ and $b \rightarrow c$ amplitudes in the former.

The ratio $\mathcal{R} \equiv \mathcal{B}(B_s^0 \rightarrow D_s^\mp K^\pm)/\mathcal{B}(B_s^0 \rightarrow D_s^- \pi^+)$ has recently been measured by LHCb [3] to be $\mathcal{R} = 0.0762 \pm 0.0015 \pm 0.0020$, where the first uncertainty is statistical and the second systematic. This is compatible with the predicted value of $\mathcal{R} = 0.086_{-0.007}^{+0.009}$ from Ref. [1], which is based on $SU(3)$ flavour symmetry and measurements from B factories. Under the same theoretical assumptions, the ratio $\mathcal{R}^* \equiv \mathcal{B}(B_s^0 \rightarrow D_s^{*\mp} K^\pm)/\mathcal{B}(B_s^0 \rightarrow D_s^{*-} \pi^+)$ is predicted to be $\mathcal{R}^* = 0.099_{-0.036}^{+0.030}$ [1] and it is therefore interesting to test this prediction for vector decays.

The $B_s^0 \rightarrow D_s^{*-} \pi^+$ and $B_s^0 \rightarrow D_s^{*\mp} K^\pm$ decays are experimentally challenging for detectors operating at hadron colliders because they require the reconstruction of a soft photon in the $D_s^{*-} \rightarrow D_s^- \gamma$ decay. This paper describes the reconstruction of the $B_s^0 \rightarrow D_s^{*-} \pi^+$ decay, previously observed by Belle [4], as well as the first observation of the $B_s^0 \rightarrow D_s^{*\mp} K^\pm$ decay and the measurement of \mathcal{R}^* . This is the first step towards a measurement of the time-dependent CP asymmetry in these decays.

The pp collision data used in this analysis correspond to an integrated luminosity of 3.0 fb^{-1} , of which 1.0 fb^{-1} were collected by LHCb in 2011 at a centre-of-mass energy of $\sqrt{s} = 7 \text{ TeV}$, and the remaining 2.0 fb^{-1} in 2012 at $\sqrt{s} = 8 \text{ TeV}$.

The ratio of branching fractions for the decays $B_s^0 \rightarrow D_s^{*\mp} K^\pm$ to $B_s^0 \rightarrow D_s^{*-} \pi^+$ is evaluated according to

$$\mathcal{R}^* = \frac{N_{K^\pm} \varepsilon_{\pi^+}}{N_{\pi^+} \varepsilon_{K^\pm}}, \quad (1)$$

where ε_X and N_X are the overall reconstruction efficiency and the observed yield, respectively, of the decay mode, and X represents either a kaon or a pion (the ‘‘bachelor’’ hadron) that accompanies the D_s^{*-} in the final state.

2 LHCb detector

The LHCb detector [5, 6] is a single-arm forward spectrometer covering the pseudorapidity range $2 < \eta < 5$, designed for the study of particles containing b or c quarks. The detector includes a high-precision tracking system consisting of a silicon-strip vertex detector surrounding the pp interaction region, a large-area silicon-strip detector located upstream of a dipole magnet with a bending power of about 4 Tm, and three stations of silicon-strip detectors and straw drift tubes placed downstream of the magnet. The tracking system provides a measurement of momentum, p , of charged particles with a relative uncertainty that varies from 0.5% at low momentum to 1.0% at 200 GeV/ c . The minimum distance of a track to a primary vertex, the impact parameter, is measured with a resolution of $(15 + 29/p_T) \mu\text{m}$, where p_T is the component of the momentum transverse to the beam, in GeV/ c . Different types of charged hadrons are distinguished using information from two ring-imaging Cherenkov detectors. Photons, electrons and hadrons are identified by a calorimeter system consisting of scintillating-pad and preshower detectors, an electromagnetic calorimeter and a hadronic calorimeter. Muons are identified

by a system composed of alternating layers of iron and multiwire proportional chambers.

The online event selection is performed by a trigger which consists of a hardware stage, based on information from the calorimeter and muon systems, followed by a software stage, which applies a full event reconstruction. At the hardware trigger stage, events are required to have a muon with high p_T or a hadron, photon or electron with high transverse energy in the calorimeters. For hadrons, the transverse energy threshold is 3.5 GeV. The software trigger requires a two-, three- or four-track secondary vertex with a significant displacement from the primary pp interaction vertices (PVs). At least one charged particle must have a transverse momentum $p_T > 1.7 \text{ GeV}/c$ and be inconsistent with originating from a PV. A multivariate algorithm [7] is used for the identification of secondary vertices consistent with the decay of a b hadron. The p_T of the photon from D_s^{*-} decay is too low to contribute to the trigger decision.

In the simulation, pp collisions are generated using PYTHIA [8] with a specific LHCb configuration [9]. Decays of hadronic particles are described by EVTGEN [10], in which final-state radiation is generated using PHOTOS [11]. The interaction of the generated particles with the detector, and its response, are implemented using the GEANT4 toolkit [12] as described in Ref. [13].

3 Event selection

Candidate B_s^0 mesons are reconstructed by combining a D_s^{*-} candidate with an additional pion or kaon of opposite charge. The preselection and selection for the two decays analysed for the measurement of \mathcal{R}^* differ only by the particle identification (PID) [14] requirements imposed on the bachelor tracks. The D_s^{*-} and D_s^- candidates are reconstructed in the $D_s^- \gamma$ and $K^- K^+ \pi^-$ decay modes, respectively. Each of the three D_s^- daughters tracks is required to have a good track quality, momentum $p > 1000 \text{ MeV}/c$, transverse momentum $p_T > 100 \text{ MeV}/c$ and a large impact parameter with respect to any PV. More stringent requirements are imposed for bachelor tracks, namely $p > 5000 \text{ MeV}/c$ and $p_T > 500 \text{ MeV}/c$. A good quality secondary vertex is required for the resulting D_s^- -bachelor combination. Photons are identified using energy deposits in the electromagnetic calorimeter that are not associated with any track in the tracking system. Due to the small difference between the masses of the D_s^{*-} and D_s^- mesons, called Δ_M in the following, the photons from the D_s^{*-} decay have an average transverse energy of a few hundred MeV/c^2 . A cut on a photon confidence level variable is used to suppress background events from hadrons, electrons and π^0 decays [6]. This confidence level variable takes into account the expected absence of matching between the calorimeter cluster and any track, the energy recorded in the preshower detector and the topology of the energy deposit in the electromagnetic and hadronic calorimeters.

Additional preselection requirements are applied to cope with a large background mainly due to genuine photons that are not D_s^{*-} decay products, or hadrons that are misidentified as photons. The reconstructed mass of the D_s^- candidate and the reconstructed Δ_M value are required to be in a $\pm 20 \text{ MeV}/c^2$ window around their known values [15]. The

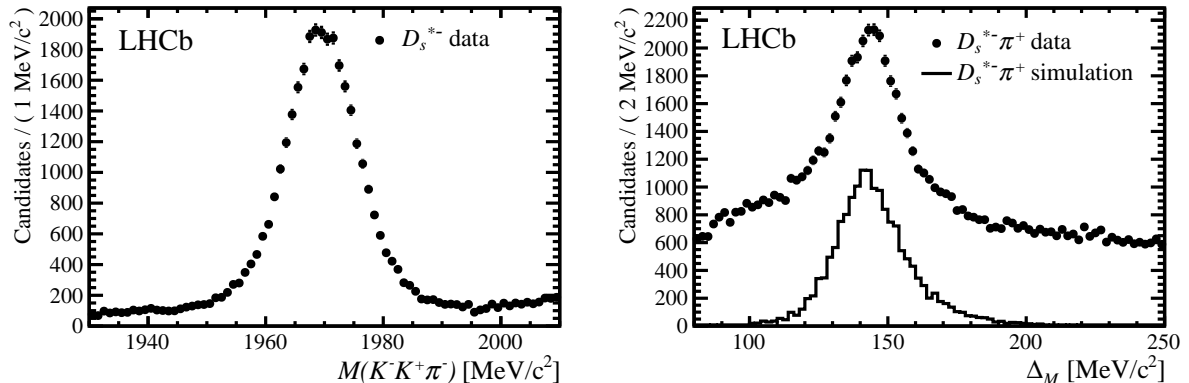


Figure 2: (left) The $K^-K^+\pi^-$ invariant mass and (right) mass difference Δ_M of the $B_s^0 \rightarrow D_s^{*-}\pi^+$ candidates. The points represent data. On the right plot the solid line represents the signal expected from the simulations.

$B_{(s)}^0 \rightarrow D_s^- K^+ (\pi^+)$ decays are vetoed by a cut on the invariant mass of the $D_s^- K^+ (\pi^+)$ system. PID requirements are applied to all final-state hadrons. Finally, the maximum distance in the η - φ plane between the D_s^- and the photon is required to satisfy $\sqrt{\Delta\eta^2 + \Delta\varphi^2} < 1$, where $\Delta\eta$ ($\Delta\varphi$) is the pseudo-rapidity (azimuthal angle) distance between the corresponding candidates.

To further reduce the combinatorial background while preserving a high signal efficiency, a multivariate approach is used. This follows closely the selection based on a boosted decision tree (BDT) [16, 17] used in the measurement of the ratio of $B_s^0 \rightarrow D_s^\mp K^\pm$ to $B_s^0 \rightarrow D_s^- \pi^+$ branching fractions [3]. The algorithm is trained with simulated $B_s^0 \rightarrow D_s^{*-}\pi^+$ events as signal, and candidates in data with an invariant mass greater than $5500 \text{ MeV}/c^2$ as background. The five variables with the highest discriminating power are found to be the B_s^0 transverse flight distance, the photon transverse momentum, the χ_{IP}^2 of the B_s^0 candidate (where χ_{IP}^2 is defined as the difference in χ^2 of the associated PV, reconstructed with and without the considered particle), the angle between the B_s^0 momentum vector and the vector connecting its production and decay vertices, and the transverse momentum of the bachelor particle. Eight additional variables, among them the transverse momenta of the remaining final-state particles, are also used. The trained algorithm is then applied to both the $B_s^0 \rightarrow D_s^{*\mp} K^\pm$ and $B_s^0 \rightarrow D_s^{*-}\pi^+$ decays.

The $M(K^-K^+\pi^-)$ and Δ_M invariant mass distributions, as obtained from the decay mode $B_s^0 \rightarrow D_s^{*-}\pi^+$, are shown in Fig. 2. These distributions have been obtained with all of the analysis requirements applied except that on the plotted variable. In both cases the B_s^0 invariant mass is restricted to a $\pm 70 \text{ MeV}/c^2$ region around the known mass. A prominent peaking structure is observed in the Δ_M distribution around $145 \text{ MeV}/c^2$, due to the radiative D_s^{*-} to D_s^- decay.

4 Signal yields

The signal yields are obtained using unbinned maximum likelihood fits to the B_s^0 candidate invariant mass distributions and are performed separately for $B_s^0 \rightarrow D_s^{*-} \pi^+$ and $B_s^0 \rightarrow D_s^{*\mp} K^\pm$ decays.

The signal shapes are parametrised by a double-sided Crystal Ball (CB) function [18], which consists of a central Gaussian part, with mean and width as parameters, and power-law tails on both lower and upper sides, to account for energy loss due to final-state radiation and detector resolution effects. The two mean values are constrained to be equal. When fitting the $D_s^{*-} \pi^+$ and $D_s^{*\mp} K^\pm$ simulated mass distributions all parameters are floated. When fitting data, the power-law tails parameters are fixed to the result of the fit to the corresponding simulation. Furthermore, both widths of the CB are set to those obtained from the signal simulation, scaled by a variable parameter in the fit to allow for differences in the mass resolution between data and simulation. The common mean of the double-sided CB is allowed to vary.

Three background categories are identified. Partially reconstructed background decays are due to B_s^0 decay modes that are similar to signal but with at least one additional photon, as for example in the case of the $B_s^0 \rightarrow D_s^{*\mp} \rho^\pm$ decays with $\rho^\pm \rightarrow \pi^0 (\rightarrow \gamma\gamma) \pi^\pm$. Fully reconstructed background events are due to B^0 decays to the same final states as the B_s^0 signal, $D_s^{*-} \pi^+$ and $D_s^{*\mp} K^\pm$. The $B_s^0 \rightarrow D_s^{*-} \pi^+$ decays gives rise to a peak in the $B_s^0 \rightarrow D_s^{*\mp} K^\pm$ decay mode when the π^+ is misidentified as a K^+ , a cross feed contribution. The cross feed due to K^\pm to π^\pm misidentification is negligible. Finally, a combinatorial background, where a genuine D_s^- meson is combined with a random (or fake) photon and a random bachelor track, can also contribute.

The number of partially and fully reconstructed background components is different for each of the two final states. The invariant mass shapes for these backgrounds are obtained from simulation and are represented in the fit as non-parametric probability density functions (PDFs). The yields of these background components are free parameters in the fit, with the exception of the $D_s^{*-} \pi^+$, $D_s^- \rho^+$ and $D_s^{*-} \rho^+$ contributions in the $D_s^{*\mp} K^\pm$ fit. The size of the $D_s^{*-} \pi^+$ cross feed is calculated from the $D_s^{*-} \pi^+$ yield and the π to K misidentification probability. The $D_s^- \rho^+$ and $D_s^{*-} \rho^+$ contributions are determined in a similar manner, summed and fixed in the fit.

To model the combinatorial background a non-parametric PDF is used. This is obtained from the events of the Δ_M sideband in the interval [185,205] MeV/ c^2 , with all other cuts unchanged.

The results of the fitting procedure applied to the two considered decay modes are shown in Fig. 3. The fitted yields are $16\,513 \pm 227$ and 1025 ± 71 for the $B_s^0 \rightarrow D_s^{*-} \pi^+$ and $B_s^0 \rightarrow D_s^{*\mp} K^\pm$ cases, respectively. When the χ^2 test is applied to gauge the quality of the fits, the latter fit has a χ^2 value of 88.5 for 100 bins and 7 free parameters, the quality of the former fit is equally good.

One of the distinctive features of the present analysis is the reconstruction of the decay mode $D_s^{*-} \rightarrow D_s^- \gamma$ at a hadron collider. The background-subtracted η and p_T distributions of these photons have been obtained using the invariant mass fit results described above

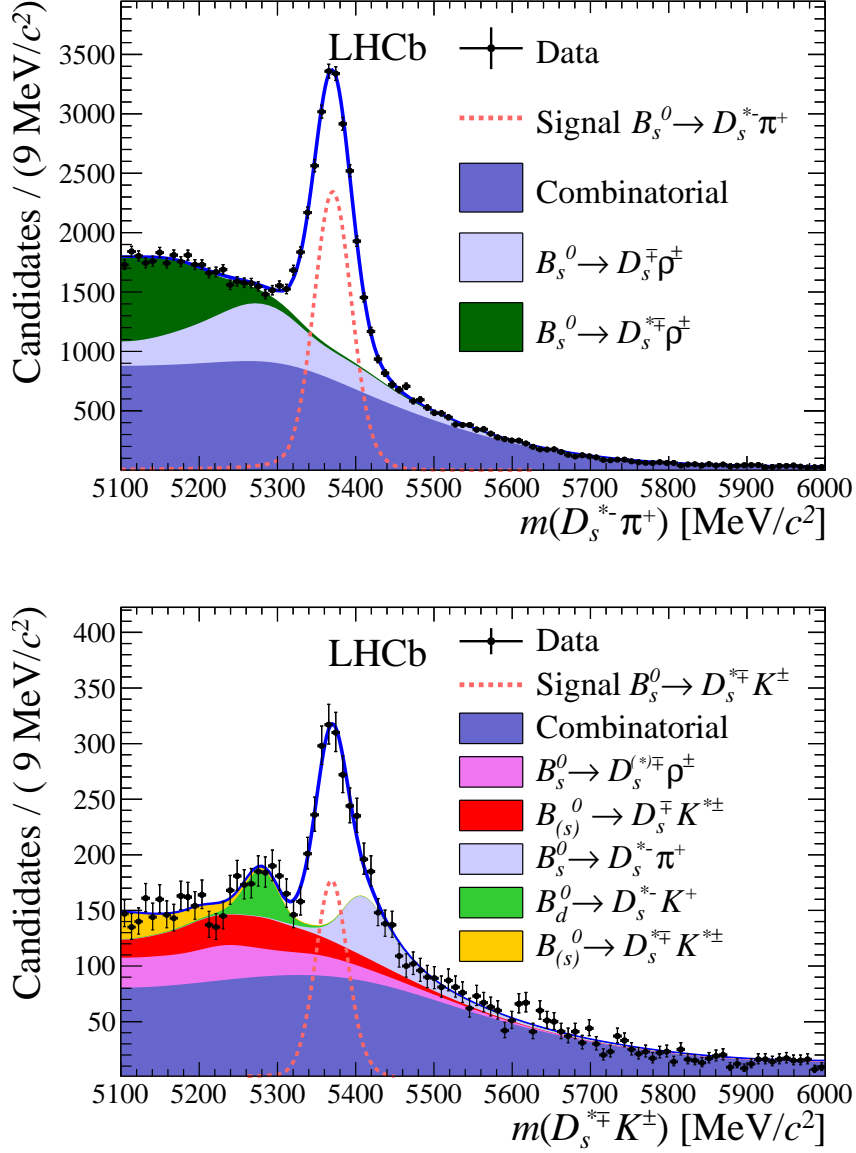


Figure 3: Invariant mass distribution of (top) $B_s^0 \rightarrow D_s^{*-} \pi^+$ and (bottom) $B_s^0 \rightarrow D_s^{*\mp} K^\pm$ candidates with fit results superimposed. The fitted signal corresponding to the first observation of $B_s^0 \rightarrow D_s^{*\mp} K^\pm$ is shown by the dotted line in the lower plot.

and the *sPlot* [19] method. These measured distributions are compared to the predictions of the simulation in Fig. 4. It is noted that most of the measured photons are very soft, with the average p_T well below $1 \text{ GeV}/c$.

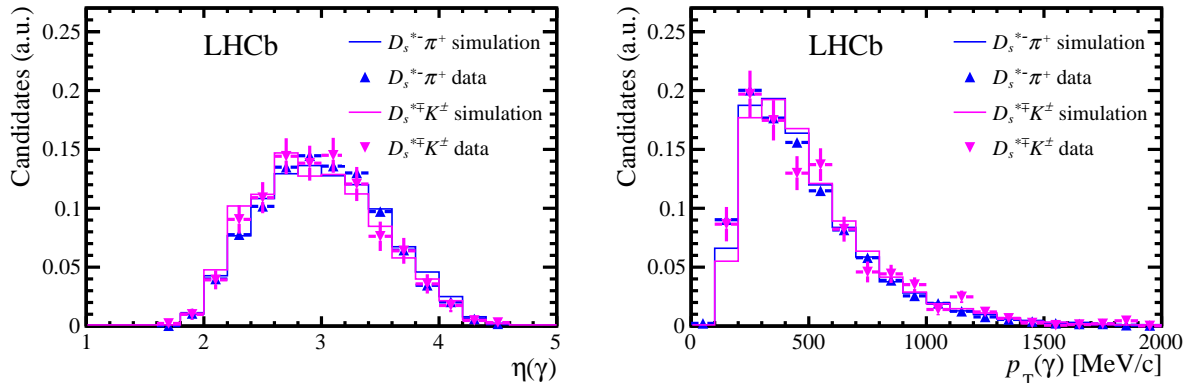


Figure 4: Distributions of (left) η and (right) p_T of the photons for the $D_s^{*-}\pi^+$ (blue) and $D_s^{*\mp}K^\pm$ (magenta) decays. Data, background-subtracted using the *sPlot* method, are represented by points, and simulations by solid lines.

5 Systematic uncertainties

Potential systematic uncertainties on \mathcal{R}^* are those due to the background modelling and the analysis selections, including the BDT and the PID cuts. Their effects are shown in Table 1 as relative variations of the final result, with their sum in quadrature assigned as the overall systematic uncertainty. The order in which the systematic uncertainties are described in the following text corresponds to successive rows in Table 1.

Combinatorial background modelling uncertainties are studied by varying the default Δ_M range used for the combinatorial background determination, $[185,205]$ MeV/ c^2 , to $[205,225]$ and $[225,245]$ MeV/ c^2 . An alternative modelling of this background, using a parametric shape obtained from the D_s^- mass sidebands, is also tested. Finally, the statistical uncertainty due to the number of events in the range $[185,205]$ MeV/ c^2 is evaluated using the bootstrap technique [20, 21]. The corresponding uncertainty is taken to be the largest spread among the four different checks.

The uncertainty due to the finite size of the simulated samples used to study the partially reconstructed backgrounds is studied using the bootstrap technique.

The uncertainties due to the $D_s^{*-}\pi^+$ cross feed and the $D_s^-\rho^+$ and $D_s^{*-}\rho^+$ contributions to the $D_s^{*\mp}K^\pm$ fit are estimated by varying their expected yields. For the $D_s^{*-}\pi^+$ cross feed the $\pm 1\sigma$ variation is obtained using the $D_s^{*-}\pi^+$ fit results. In the $D_s^-\rho^+$ and $D_s^{*-}\rho^+$ cases the branching ratio uncertainties and photon kinematic distributions are different from the $D_s^{*-}\pi^+$ ones so the uncertainty in the yields are large. These yields are conservatively varied by $\pm 50\%$. The observed differences in the final result are assigned as the systematic uncertainties associated with these sources.

The systematic uncertainty associated with the BDT is studied by reweighting the simulation to improve the agreement with data [3].

The π and K PID efficiencies used for the bachelor track have been extracted from

a $D^{*+} \rightarrow D^0\pi^+$ calibration sample and parametrized as a function of several kinematic quantities of these tracks. The uncertainties in this procedure, propagated to the final result, lead to the PID systematic uncertainty.

The systematic uncertainty from the hardware trigger efficiency arises from differences in the pion and kaon trigger efficiencies which are not reproduced in the simulation [22]. The uncertainty is scaled with the fraction of events where a signal track was responsible for triggering.

Table 1: Estimated systematic uncertainties on \mathcal{R}^* .

source	relative variation (%)
combinatorial background	+4.7 -2.2
simulation sample size	± 1.4
$D_s^{*-}\pi^+$ cross feed	± 0.8
$D_s^{(*)-}\rho^+$ “cross feed”	+0 -1.6
BDT	± 0.5
PID uncertainties	± 1.0
hardware trigger	± 1.0
total	+5.2 -3.5

6 Results

The ratio of branching fractions, measured in this analysis for the first time, is

$$\mathcal{R}^* \equiv \mathcal{B}(B_s^0 \rightarrow D_s^{*\mp}K^\pm)/\mathcal{B}(B_s^0 \rightarrow D_s^{*-}\pi^+) = 0.068 \pm 0.005 \text{ (stat)} \begin{matrix} +0.003 \\ -0.002 \end{matrix} \text{ (syst)},$$

where the overall systematic uncertainty is mainly due to the uncertainty on the combinatorial background estimate. The result for \mathcal{R}^* differs from the uncorrected $B_s^0 \rightarrow D_s^{*\mp}K^\pm$ to $B_s^0 \rightarrow D_s^{*-}\pi^+$ events ratio by a factor depending on the simulation and the PID efficiencies. This factor is determined to be 1.095 ± 0.016 and is dominated by the K to π PID efficiency ratio.

The measured value of \mathcal{R}^* is consistent with the theoretical prediction of $\mathcal{R}^* = 0.099_{-0.036}^{+0.030}$ [1], within the very large uncertainty of the latter. The theory is found to provide a good description of the measurements for both \mathcal{R}^* and \mathcal{R} [3]. Other theoretical predictions of \mathcal{R}^* have been published in Refs. [23–27].

Combining the measured value of \mathcal{R}^* with the value of $\mathcal{B}(B_s^0 \rightarrow D_s^{*-}\pi^+)$ obtained by Belle [4] leads to

$$\mathcal{B}(B_s^0 \rightarrow D_s^{*\mp}K^\pm) = (16.3 \pm 1.2 \text{ (stat)} \begin{matrix} +0.7 \\ -0.5 \end{matrix} \text{ (syst)} \pm 4.8 \text{ (norm)}) \times 10^{-5},$$

where the uncertainties are statistical, systematic and due to the uncertainty on $\mathcal{B}(B_s^0 \rightarrow D_s^{*-}\pi^+)$.

Acknowledgements

We express our gratitude to our colleagues in the CERN accelerator departments for the excellent performance of the LHC. We thank the technical and administrative staff at the LHCb institutes. We acknowledge support from CERN and from the national agencies: CAPES, CNPq, FAPERJ and FINEP (Brazil); NSFC (China); CNRS/IN2P3 (France); BMBF, DFG, HGF and MPG (Germany); INFN (Italy); FOM and NWO (The Netherlands); MNiSW and NCN (Poland); MEN/IFA (Romania); MinES and FANO (Russia); MinECo (Spain); SNSF and SER (Switzerland); NASU (Ukraine); STFC (United Kingdom); NSF (USA). The Tier1 computing centres are supported by IN2P3 (France), KIT and BMBF (Germany), INFN (Italy), NWO and SURF (The Netherlands), PIC (Spain), GridPP (United Kingdom). We are indebted to the communities behind the multiple open source software packages on which we depend. We are also thankful for the computing resources and the access to software R&D tools provided by Yandex LLC (Russia). Individual groups or members have received support from EPLANET, Marie Skłodowska-Curie Actions and ERC (European Union), Conseil général de Haute-Savoie, Labex ENIGMASS and OCEVU, Région Auvergne (France), RFBR (Russia), XuntaGal and GENCAT (Spain), Royal Society and Royal Commission for the Exhibition of 1851 (United Kingdom).

References

- [1] K. De Bruyn *et al.*, *Exploring $B_s \rightarrow D_s^{(*)\pm} K^\mp$ decays in the presence of a sizable width difference $\Delta\Gamma_s$* , Nucl. Phys. **B868** (2012) 351, [arXiv:1208.6463](#).
- [2] LHCb collaboration, R. Aaij *et al.*, *Measurement of CP asymmetry in $B_s^0 \rightarrow D_s^\mp K^\pm$ decays*, JHEP **11** (2014) 060, [arXiv:1407.6127](#).
- [3] LHCb collaboration, R. Aaij *et al.*, *Determination of the branching fractions of $B_s^0 \rightarrow D_s^\mp K^\pm$ and $B^0 \rightarrow D_s^- K^+$* , [arXiv:1412.7654](#), submitted to JHEP.
- [4] Belle collaboration, R. Louvot *et al.*, *Observation of $B_s^0 \rightarrow D_s^{*-} \pi^+$ and $B_s^0 \rightarrow D_s^{(*)-} \rho^+$ and measurement of the $B_s^0 \rightarrow D_s^{*-} \rho^+$ longitudinal polarization fraction*, Phys. Rev. Lett **104** (2010) 231801, [arXiv:1003.5312](#).
- [5] LHCb collaboration, A. A. Alves Jr. *et al.*, *The LHCb detector at the LHC*, JINST **3** (2008) S08005.
- [6] LHCb collaboration, R. Aaij *et al.*, *LHCb detector performance*, Int. J. Mod. Phys. **A30** (2015) 1530022, [arXiv:1412.6352](#).
- [7] V. V. Gligorov and M. Williams, *Efficient, reliable and fast high-level triggering using a bonsai boosted decision tree*, JINST **8** (2013) P02013, [arXiv:1210.6861](#).

- [8] T. Sjöstrand, S. Mrenna, and P. Skands, *PYTHIA 6.4 physics and manual*, JHEP **05** (2006) 026, [arXiv:hep-ph/0603175](#); T. Sjöstrand, S. Mrenna, and P. Skands, *A brief introduction to PYTHIA 8.1*, Comput. Phys. Commun. **178** (2008) 852, [arXiv:0710.3820](#).
- [9] I. Belyaev *et al.*, *Handling of the generation of primary events in Gauss, the LHCb simulation framework*, J. Phys. Conf. Ser. **331** (2011) 032047.
- [10] D. J. Lange, *The EvtGen particle decay simulation package*, Nucl. Instrum. Meth. **A462** (2001) 152.
- [11] P. Golonka and Z. Was, *PHOTOS Monte Carlo: A precision tool for QED corrections in Z and W decays*, Eur. Phys. J. **C45** (2006) 97, [arXiv:hep-ph/0506026](#).
- [12] Geant4 collaboration, J. Allison *et al.*, *Geant4 developments and applications*, IEEE Trans. Nucl. Sci. **53** (2006) 270; Geant4 collaboration, S. Agostinelli *et al.*, *Geant4: A simulation toolkit*, Nucl. Instrum. Meth. **A506** (2003) 250.
- [13] M. Clemencic *et al.*, *The LHCb simulation application, Gauss: Design, evolution and experience*, J. Phys. Conf. Ser. **331** (2011) 032023.
- [14] M. Adinolfi *et al.*, *Performance of the LHCb RICH detector at the LHC*, Eur. Phys. J. **C73** (2013) 2431, [arXiv:1211.6759](#).
- [15] Particle Data Group, K. A. Olive *et al.*, *Review of particle physics*, Chin. Phys. **C38** (2014) 090001.
- [16] L. Breiman, J. H. Friedman, R. A. Olshen, and C. J. Stone, *Classification and regression trees*, Wadsworth international group, Belmont, California, USA, 1984.
- [17] R. E. Schapire and Y. Freund, *A decision-theoretic generalization of on-line learning and an application to boosting*, Jour. Comp. and Syst. Sc. **55** (1997) 119.
- [18] T. Skwarnicki, *A study of the radiative cascade transitions between the Upsilon-prime and Upsilon resonances*, PhD thesis, Institute of Nuclear Physics, Krakow, 1986, DESY-F31-86-02.
- [19] M. Pivk and F. R. Le Diberder, *sPlot: A statistical tool to unfold data distributions*, Nucl. Instrum. Meth. **A555** (2005) 356, [arXiv:physics/0402083](#).
- [20] B. Efron, *Bootstrap methods: Another look at the jackknife*, The Annals of Statistics **7** (1979) 1.
- [21] I. Narsky and F. Porter, *Statistical analysis techniques in particle physics*, Wiley-VCH, 2013.
- [22] A. Martin Sanchez, P. Robbe, and M.-H. Schune, *Performances of the LHCb L0 Calorimeter Trigger*, Jun, 2012. LHCb-PUB-2011-026.

- [23] P. Blasi, P. Colangelo, G. Nardulli, and N. Paver, *Phenomenology of B_s decays*, Phys. Rev. D **49** (1994) 238, [arXiv:9307.290](#).
- [24] R. H. Li, C. D. Lu, and H. Zou, *The $B(B_s) \rightarrow D_{(s)}P$, $D_{(s)}V$, $D_{(s)}^*P$ and $D_{(s)}^*V$ decays in the perturbative QCD approach*, Phys. Rev. D **78** (2008) 14018, [arXiv:0803.1073](#).
- [25] K. Azizi, R. Khosravi, and F. Falahati, *Analysis of the $B_q \rightarrow D_q(D_q^*)P$ and $B_q \rightarrow D_q(D_q^*)V$ decays within the factorization approach in QCD*, Int. J. Mod. Phys. A **24** (2009) 5845, [arXiv:0811.2671](#).
- [26] X. J. Chen, H. F. Fu, C. S. Kim, and G. L. Wang, *Estimating form factors of $B_s \rightarrow D_s^{(*)}$ and their applications to semi-leptonic and non-leptonic decays*, Nucl. Part. Phys. **39** (2012) 45002, [arXiv:1106.3003](#).
- [27] R. N. Faustov and V. O. Galkin, *Weak decays of B_s mesons to D_s in the relativistic quark model*, Phys. Rev. D **87** (2012) 34033, [arXiv:1212.3167](#).

LHCb collaboration

R. Aaij⁴¹, B. Adeva³⁷, M. Adinolfi⁴⁶, A. Affolder⁵², Z. Ajaltouni⁵, S. Akar⁶, J. Albrecht⁹, F. Alessio³⁸, M. Alexander⁵¹, S. Ali⁴¹, G. Alkhazov³⁰, P. Alvarez Cartelle⁵³, A.A. Alves Jr⁵⁷, S. Amato², S. Amerio²², Y. Amhis⁷, L. An³, L. Anderlini^{17,g}, J. Anderson⁴⁰, M. Andreotti^{16,f}, J.E. Andrews⁵⁸, R.B. Appleby⁵⁴, O. Aquines Gutierrez¹⁰, F. Archilli³⁸, A. Artamonov³⁵, M. Artuso⁵⁹, E. Aslanides⁶, G. Auriemma^{25,n}, M. Baalouch⁵, S. Bachmann¹¹, J.J. Back⁴⁸, A. Badalov³⁶, C. Baesso⁶⁰, W. Baldini^{16,38}, R.J. Barlow⁵⁴, C. Barschel³⁸, S. Barsuk⁷, W. Barter³⁸, V. Batozskaya²⁸, V. Battista³⁹, A. Bay³⁹, L. Beaucourt⁴, J. Beddow⁵¹, F. Bedeschi²³, I. Bediaga¹, L.J. Bel⁴¹, I. Belyaev³¹, E. Ben-Haim⁸, G. Bencivenni¹⁸, S. Benson³⁸, J. Benton⁴⁶, A. Berezhnoy³², R. Bernet⁴⁰, A. Bertolin²², M.-O. Bettler³⁸, M. van Beuzekom⁴¹, A. Bien¹¹, S. Bifani⁴⁵, T. Bird⁵⁴, A. Bizzeti^{17,i}, T. Blake⁴⁸, F. Blanc³⁹, J. Blouw¹⁰, S. Blusk⁵⁹, V. Bocci²⁵, A. Bondar³⁴, N. Bondar^{30,38}, W. Bonivento¹⁵, S. Borghi⁵⁴, M. Borsato⁷, T.J.V. Bowcock⁵², E. Bowen⁴⁰, C. Bozzi¹⁶, S. Braun¹¹, D. Brett⁵⁴, M. Britsch¹⁰, T. Britton⁵⁹, J. Brodzicka⁵⁴, N.H. Brook⁴⁶, A. Bursche⁴⁰, J. Buytaert³⁸, S. Cadeddu¹⁵, R. Calabrese^{16,f}, M. Calvi^{20,k}, M. Calvo Gomez^{36,p}, P. Campana¹⁸, D. Campora Perez³⁸, L. Capriotti⁵⁴, A. Carbone^{14,d}, G. Carboni^{24,l}, R. Cardinale^{19,j}, A. Cardini¹⁵, P. Carniti²⁰, L. Carson⁵⁰, K. Carvalho Akiba^{2,38}, R. Casanova Mohr³⁶, G. Casse⁵², L. Cassina^{20,k}, L. Castillo Garcia³⁸, M. Cattaneo³⁸, Ch. Cauet⁹, G. Cavallero¹⁹, R. Cenci^{23,t}, M. Charles⁸, Ph. Charpentier³⁸, M. Chefdeville⁴, S. Chen⁵⁴, S.-F. Cheung⁵⁵, N. Chiapolini⁴⁰, M. Chrzaszcz^{40,26}, X. Cid Vidal³⁸, G. Ciezarek⁴¹, P.E.L. Clarke⁵⁰, M. Clemencic³⁸, H.V. Cliff⁴⁷, J. Closier³⁸, V. Coco³⁸, J. Cogan⁶, E. Cogneras⁵, V. Cogoni^{15,e}, L. Cojocariu²⁹, G. Collazuol²², P. Collins³⁸, A. Comerma-Montells¹¹, A. Contu^{15,38}, A. Cook⁴⁶, M. Coombes⁴⁶, S. Coquereau⁸, G. Corti³⁸, M. Corvo^{16,f}, B. Couturier³⁸, G.A. Cowan⁵⁰, D.C. Craik⁴⁸, A. Crocombe⁴⁸, M. Cruz Torres⁶⁰, S. Cunliffe⁵³, R. Currie⁵³, C. D'Ambrosio³⁸, J. Dalseno⁴⁶, P.N.Y. David⁴¹, A. Davis⁵⁷, K. De Bruyn⁴¹, S. De Capua⁵⁴, M. De Cian¹¹, J.M. De Miranda¹, L. De Paula², W. De Silva⁵⁷, P. De Simone¹⁸, C.-T. Dean⁵¹, D. Decamp⁴, M. Deckenhoff⁹, L. Del Buono⁸, N. Déléage⁴, D. Derkach⁵⁵, O. Deschamps⁵, F. Dettori³⁸, B. Dey⁴⁰, A. Di Canto³⁸, F. Di Ruscio²⁴, H. Dijkstra³⁸, S. Donleavy⁵², F. Dordei¹¹, M. Dorigo³⁹, A. Dosil Suárez³⁷, D. Dossett⁴⁸, A. Dovbnya⁴³, K. Dreimanic⁵², G. Dujany⁵⁴, F. Dupertuis³⁹, P. Durante³⁸, R. Dzhelyadin³⁵, A. Dziurda²⁶, A. Dzyuba³⁰, S. Easo^{49,38}, U. Egede⁵³, V. Egorychev³¹, S. Eidelman³⁴, S. Eisenhardt⁵⁰, U. Eitschberger⁹, R. Ekelhof⁹, L. Eklund⁵¹, I. El Rifai⁵, Ch. Elsasser⁴⁰, S. Ely⁵⁹, S. Esen¹¹, H.M. Evans⁴⁷, T. Evans⁵⁵, A. Falabella¹⁴, C. Färber¹¹, C. Farinelli⁴¹, N. Farley⁴⁵, S. Farry⁵², R. Fay⁵², D. Ferguson⁵⁰, V. Fernandez Albor³⁷, F. Ferrari¹⁴, F. Ferreira Rodrigues¹, M. Ferro-Luzzi³⁸, S. Filippov³³, M. Fiore^{16,38,f}, M. Fiorini^{16,f}, M. Firlej²⁷, C. Fitzpatrick³⁹, T. Fiutowski²⁷, P. Fol⁵³, M. Fontana¹⁰, F. Fontanelli^{19,j}, R. Forty³⁸, O. Francisco², M. Frank³⁸, C. Frei³⁸, M. Frosini¹⁷, J. Fu^{21,38}, E. Furfaro^{24,l}, A. Gallas Torreira³⁷, D. Galli^{14,d}, S. Gallorini^{22,38}, S. Gambetta^{19,j}, M. Gandelman², P. Gandini⁵⁵, Y. Gao³, J. García Pardiñas³⁷, J. Garofoli⁵⁹, J. Garra Tico⁴⁷, L. Garrido³⁶, D. Gascon³⁶, C. Gaspar³⁸, U. Gastaldi¹⁶, R. Gauld⁵⁵, L. Gavardi⁹, G. Gazzoni⁵, A. Geraci^{21,v}, D. Gerick¹¹, E. Gersabeck¹¹, M. Gersabeck⁵⁴, T. Gershon⁴⁸, Ph. Ghez⁴, A. Gianelle²², S. Giani³⁹, V. Gibson⁴⁷, L. Giubega²⁹, V.V. Gligorov³⁸, C. Göbel⁶⁰, D. Golubkov³¹, A. Golutvin^{53,31,38}, A. Gomes^{1,a}, C. Gotti^{20,k}, M. Grabalosa Gándara⁵, R. Graciani Diaz³⁶, L.A. Granado Cardoso³⁸, E. Graugés³⁶, E. Graverini⁴⁰, G. Graziani¹⁷, A. Grecu²⁹, E. Greening⁵⁵, S. Gregson⁴⁷, P. Griffith⁴⁵, L. Grillo¹¹, O. Grünberg⁶³, B. Gui⁵⁹, E. Gushchin³³, Yu. Guz^{35,38}, T. Gys³⁸, C. Hadjivasiliou⁵⁹, G. Haefeli³⁹, C. Haen³⁸, S.C. Haines⁴⁷, S. Hall⁵³,

B. Hamilton⁵⁸, T. Hampson⁴⁶, X. Han¹¹, S. Hansmann-Menzemer¹¹, N. Harnew⁵⁵,
 S.T. Harnew⁴⁶, J. Harrison⁵⁴, J. He³⁸, T. Head³⁹, V. Heijne⁴¹, K. Hennessy⁵², P. Henrard⁵,
 L. Henry⁸, J.A. Hernando Morata³⁷, E. van Herwijnen³⁸, M. Heß⁶³, A. Hicheur², D. Hill⁵⁵,
 M. Hoballah⁵, C. Hombach⁵⁴, W. Hulsbergen⁴¹, T. Humair⁵³, N. Hussain⁵⁵, D. Hutchcroft⁵²,
 D. Hynds⁵¹, M. Idzik²⁷, P. Ilten⁵⁶, R. Jacobsson³⁸, A. Jaeger¹¹, J. Jalocha⁵⁵, E. Jans⁴¹,
 A. Jawahery⁵⁸, F. Jing³, M. John⁵⁵, D. Johnson³⁸, C.R. Jones⁴⁷, C. Joram³⁸, B. Jost³⁸,
 N. Jurik⁵⁹, S. Kandybei⁴³, W. Kanso⁶, M. Karacson³⁸, T.M. Karbach³⁸, S. Karodia⁵¹,
 M. Kelsey⁵⁹, I.R. Kenyon⁴⁵, M. Kenzie³⁸, T. Ketel⁴², B. Khanji^{20,38,k}, C. Khurewathanakul³⁹,
 S. Klaver⁵⁴, K. Klimaszewski²⁸, O. Kochebina⁷, M. Kolpin¹¹, I. Komarov³⁹, R.F. Koopman⁴²,
 P. Koppenburg^{41,38}, M. Korolev³², L. Kravchuk³³, K. Kreplin¹¹, M. Kreps⁴⁸, G. Krocker¹¹,
 P. Krokovny³⁴, F. Kruse⁹, W. Kucewicz^{26,o}, M. Kucharczyk²⁶, V. Kudryavtsev³⁴, K. Kurek²⁸,
 T. Kvaratskheliya³¹, V.N. La Thi³⁹, D. Lacarrere³⁸, G. Lafferty⁵⁴, A. Lai¹⁵, D. Lambert⁵⁰,
 R.W. Lambert⁴², G. Lanfranchi¹⁸, C. Langenbruch⁴⁸, B. Langhans³⁸, T. Latham⁴⁸,
 C. Lazzeroni⁴⁵, R. Le Gac⁶, J. van Leerdam⁴¹, J.-P. Lees⁴, R. Lefèvre⁵, A. Leflat³²,
 J. Lefrançois⁷, O. Leroy⁶, T. Lesiak²⁶, B. Leverington¹¹, Y. Li⁷, T. Likhomanenko^{65,64},
 M. Liles⁵², R. Lindner³⁸, C. Linn³⁸, F. Lionetto⁴⁰, B. Liu¹⁵, S. Lohn³⁸, I. Longstaff⁵¹,
 J.H. Lopes², P. Lowdon⁴⁰, D. Lucchesi^{22,r}, H. Luo⁵⁰, A. Lupato²², E. Luppi^{16,f}, O. Lupton⁵⁵,
 F. Machefert⁷, F. Maciuc²⁹, O. Maev³⁰, S. Malde⁵⁵, A. Malinin⁶⁴, G. Manca^{15,e}, G. Mancinelli⁶,
 P. Manning⁵⁹, A. Mapelli³⁸, J. Maratas⁵, J.F. Marchand⁴, U. Marconi¹⁴, C. Marin Benito³⁶,
 P. Marino^{23,38,t}, R. Märki³⁹, J. Marks¹¹, G. Martellotti²⁵, M. Martinelli³⁹, D. Martinez Santos⁴²,
 F. Martinez Vidal⁶⁶, D. Martins Tostes², A. Massafferri¹, R. Matev³⁸, A. Mathad⁴⁸, Z. Mathe³⁸,
 C. Matteuzzi²⁰, A. Mauri⁴⁰, B. Maurin³⁹, A. Mazurov⁴⁵, M. McCann⁵³, J. McCarthy⁴⁵,
 A. McNab⁵⁴, R. McNulty¹², B. Meadows⁵⁷, F. Meier⁹, M. Meissner¹¹, M. Merk⁴¹,
 D.A. Milanes⁶², M.-N. Minard⁴, D.S. Mitzel¹¹, J. Molina Rodriguez⁶⁰, S. Monteil⁵,
 M. Morandin²², P. Morawski²⁷, A. Mordà⁶, M.J. Morello^{23,t}, J. Moron²⁷, A.-B. Morris⁵⁰,
 R. Mountain⁵⁹, F. Muheim⁵⁰, K. Müller⁴⁰, M. Mussini¹⁴, B. Muster³⁹, P. Naik⁴⁶, T. Nakada³⁹,
 R. Nandakumar⁴⁹, I. Nasteva², M. Needham⁵⁰, N. Neri²¹, S. Neubert¹¹, N. Neufeld³⁸,
 M. Neuner¹¹, A.D. Nguyen³⁹, T.D. Nguyen³⁹, C. Nguyen-Mau^{39,q}, V. Niess⁵, R. Niet⁹,
 N. Nikitin³², T. Nikodem¹¹, A. Novoselov³⁵, D.P. O'Hanlon⁴⁸, A. Oblakowska-Mucha²⁷,
 V. Obraztsov³⁵, S. Ogilvy⁵¹, O. Okhrimenko⁴⁴, R. Oldeman^{15,e}, C.J.G. Onderwater⁶⁷,
 B. Osorio Rodrigues¹, J.M. Otalora Goicochea², A. Otto³⁸, P. Owen⁵³, A. Oyanguren⁶⁶,
 A. Palano^{13,c}, F. Palombo^{21,u}, M. Palutan¹⁸, J. Panman³⁸, A. Papanestis⁴⁹, M. Pappagallo⁵¹,
 L.L. Pappalardo^{16,f}, C. Parkes⁵⁴, G. Passaleva¹⁷, G.D. Patel⁵², M. Patel⁵³, C. Patrignani^{19,j},
 A. Pearce^{54,49}, A. Pellegrino⁴¹, G. Penso^{25,m}, M. Pepe Altarelli³⁸, S. Perazzini^{14,d}, P. Perret⁵,
 L. Pescatore⁴⁵, K. Petridis⁴⁶, A. Petrolini^{19,j}, E. Picatoste Olloqui³⁶, B. Pietrzyk⁴, T. Pilar⁴⁸,
 D. Pinci²⁵, A. Pistone¹⁹, S. Playfer⁵⁰, M. Plo Casasus³⁷, T. Poikela³⁸, F. Polci⁸,
 A. Poluektov^{48,34}, I. Polyakov³¹, E. Polcarpo², A. Popov³⁵, D. Popov¹⁰, B. Popovici²⁹,
 C. Potterat², E. Price⁴⁶, J.D. Price⁵², J. Prisciandaro³⁹, A. Pritchard⁵², C. Prouve⁴⁶,
 V. Pugatch⁴⁴, A. Puig Navarro³⁹, G. Punzi^{23,s}, W. Qian⁴, R. Quagliani^{7,46}, B. Rachwal²⁶,
 J.H. Rademacker⁴⁶, B. Rakotomiaramanana³⁹, M. Rama²³, M.S. Rangel², I. Raniuk⁴³,
 N. Rauschmayr³⁸, G. Raven⁴², F. Redi⁵³, S. Reichert⁵⁴, M.M. Reid⁴⁸, A.C. dos Reis¹,
 S. Ricciardi⁴⁹, S. Richards⁴⁶, M. Rihl³⁸, K. Rinnert⁵², V. Rives Molina³⁶, P. Robbe^{7,38},
 A.B. Rodrigues¹, E. Rodrigues⁵⁴, J.A. Rodriguez Lopez⁶², P. Rodriguez Perez⁵⁴, S. Roiser³⁸,
 V. Romanovsky³⁵, A. Romero Vidal³⁷, M. Rotondo²², J. Rouvinet³⁹, T. Ruf³⁸, H. Ruiz³⁶,
 P. Ruiz Valls⁶⁶, J.J. Saborido Silva³⁷, N. Sagidova³⁰, P. Sail⁵¹, B. Saitta^{15,e},
 V. Salustino Guimaraes², C. Sanchez Mayordomo⁶⁶, B. Sanmartin Sedes³⁷, R. Santacesaria²⁵,

C. Santamarina Rios³⁷, E. Santovetti^{24,l}, A. Sarti^{18,m}, C. Satriano^{25,n}, A. Satta²⁴,
D.M. Saunders⁴⁶, D. Savrina^{31,32}, M. Schiller³⁸, H. Schindler³⁸, M. Schlupp⁹, M. Schmelling¹⁰,
B. Schmidt³⁸, O. Schneider³⁹, A. Schopper³⁸, M.-H. Schune⁷, R. Schwemmer³⁸, B. Sciascia¹⁸,
A. Sciubba^{25,m}, A. Semennikov³¹, I. Sepp⁵³, N. Serra⁴⁰, J. Serrano⁶, L. Sestini²², P. Seyfert¹¹,
M. Shapkin³⁵, I. Shapoval^{16,43,f}, Y. Shcheglov³⁰, T. Shears⁵², L. Shekhtman³⁴, V. Shevchenko⁶⁴,
A. Shires⁹, R. Silva Coutinho⁴⁸, G. Simi²², M. Sirendi⁴⁷, N. Skidmore⁴⁶, I. Skillicorn⁵¹,
T. Skwarnicki⁵⁹, E. Smith^{55,49}, E. Smith⁵³, J. Smith⁴⁷, M. Smith⁵⁴, H. Snoek⁴¹,
M.D. Sokoloff^{57,38}, F.J.P. Soler⁵¹, F. Soomro³⁹, D. Souza⁴⁶, B. Souza De Paula², B. Spaan⁹,
P. Spradlin⁵¹, S. Sridharan³⁸, F. Stagni³⁸, M. Stahl¹¹, S. Stahl³⁸, O. Steinkamp⁴⁰,
O. Stenyakin³⁵, F. Sterpka⁵⁹, S. Stevenson⁵⁵, S. Stoica²⁹, S. Stone⁵⁹, B. Storaci⁴⁰, S. Stracka^{23,t},
M. Straticiu²⁹, U. Straumann⁴⁰, R. Stroili²², L. Sun⁵⁷, W. Sutcliffe⁵³, K. Swientek²⁷,
S. Swientek⁹, V. Syropoulos⁴², M. Szczekowski²⁸, P. Szczypka^{39,38}, T. Szumlak²⁷,
S. T'Jampens⁴, M. Teklishyn⁷, G. Tellarini^{16,f}, F. Teubert³⁸, C. Thomas⁵⁵, E. Thomas³⁸,
J. van Tilburg⁴¹, V. Tisserand⁴, M. Tobin³⁹, J. Todd⁵⁷, S. Tolk⁴², L. Tomassetti^{16,f},
D. Tonelli³⁸, S. Topp-Joergensen⁵⁵, N. Torr⁵⁵, E. Tournefier⁴, S. Tourneur³⁹, K. Trabelsi³⁹,
M.T. Tran³⁹, M. Tresch⁴⁰, A. Trisovic³⁸, A. Tsaregorodtsev⁶, P. Tsopelas⁴¹, N. Tuning^{41,38},
A. Ukleja²⁸, A. Ustyuzhanin^{65,64}, U. Uwer¹¹, C. Vacca^{15,e}, V. Vagnoni¹⁴, G. Valenti¹⁴,
A. Vallier⁷, R. Vazquez Gomez¹⁸, P. Vazquez Regueiro³⁷, C. Vázquez Sierra³⁷, S. Vecchi¹⁶,
J.J. Velthuis⁴⁶, M. Veltri^{17,h}, G. Veneziano³⁹, M. Vesterinen¹¹, J.V. Viana Barbosa³⁸, B. Viaud⁷,
D. Vieira², M. Vieites Diaz³⁷, X. Vilasis-Cardona^{36,p}, A. Vollhardt⁴⁰, D. Volyanskyy¹⁰,
D. Voong⁴⁶, A. Vorobyev³⁰, V. Vorobyev³⁴, C. Voß⁶³, J.A. de Vries⁴¹, R. Waldi⁶³, C. Wallace⁴⁸,
R. Wallace¹², J. Walsh²³, S. Wandernoth¹¹, J. Wang⁵⁹, D.R. Ward⁴⁷, N.K. Watson⁴⁵,
D. Websdale⁵³, A. Weiden⁴⁰, M. Whitehead⁴⁸, D. Wiedner¹¹, G. Wilkinson^{55,38}, M. Wilkinson⁵⁹,
M. Williams³⁸, M.P. Williams⁴⁵, M. Williams⁵⁶, F.F. Wilson⁴⁹, J. Wimberley⁵⁸, J. Wishahi⁹,
W. Wislicki²⁸, M. Witek²⁶, G. Wormser⁷, S.A. Wotton⁴⁷, S. Wright⁴⁷, K. Wyllie³⁸, Y. Xie⁶¹,
Z. Xu³⁹, Z. Yang³, X. Yuan³⁴, O. Yushchenko³⁵, M. Zangoli¹⁴, M. Zavertyaev^{10,b}, L. Zhang³,
Y. Zhang³, A. Zhelezov¹¹, A. Zhokhov³¹, L. Zhong³.

¹ Centro Brasileiro de Pesquisas Físicas (CBPF), Rio de Janeiro, Brazil

² Universidade Federal do Rio de Janeiro (UFRJ), Rio de Janeiro, Brazil

³ Center for High Energy Physics, Tsinghua University, Beijing, China

⁴ LAPP, Université Savoie Mont-Blanc, CNRS/IN2P3, Annecy-Le-Vieux, France

⁵ Clermont Université, Université Blaise Pascal, CNRS/IN2P3, LPC, Clermont-Ferrand, France

⁶ CPPM, Aix-Marseille Université, CNRS/IN2P3, Marseille, France

⁷ LAL, Université Paris-Sud, CNRS/IN2P3, Orsay, France

⁸ LPNHE, Université Pierre et Marie Curie, Université Paris Diderot, CNRS/IN2P3, Paris, France

⁹ Fakultät Physik, Technische Universität Dortmund, Dortmund, Germany

¹⁰ Max-Planck-Institut für Kernphysik (MPIK), Heidelberg, Germany

¹¹ Physikalisches Institut, Ruprecht-Karls-Universität Heidelberg, Heidelberg, Germany

¹² School of Physics, University College Dublin, Dublin, Ireland

¹³ Sezione INFN di Bari, Bari, Italy

¹⁴ Sezione INFN di Bologna, Bologna, Italy

¹⁵ Sezione INFN di Cagliari, Cagliari, Italy

¹⁶ Sezione INFN di Ferrara, Ferrara, Italy

¹⁷ Sezione INFN di Firenze, Firenze, Italy

¹⁸ Laboratori Nazionali dell'INFN di Frascati, Frascati, Italy

¹⁹ Sezione INFN di Genova, Genova, Italy

²⁰ Sezione INFN di Milano Bicocca, Milano, Italy

²¹ Sezione INFN di Milano, Milano, Italy

- ²² *Sezione INFN di Padova, Padova, Italy*
- ²³ *Sezione INFN di Pisa, Pisa, Italy*
- ²⁴ *Sezione INFN di Roma Tor Vergata, Roma, Italy*
- ²⁵ *Sezione INFN di Roma La Sapienza, Roma, Italy*
- ²⁶ *Henryk Niewodniczanski Institute of Nuclear Physics Polish Academy of Sciences, Kraków, Poland*
- ²⁷ *AGH - University of Science and Technology, Faculty of Physics and Applied Computer Science, Kraków, Poland*
- ²⁸ *National Center for Nuclear Research (NCBJ), Warsaw, Poland*
- ²⁹ *Horia Hulubei National Institute of Physics and Nuclear Engineering, Bucharest-Magurele, Romania*
- ³⁰ *Petersburg Nuclear Physics Institute (PNPI), Gatchina, Russia*
- ³¹ *Institute of Theoretical and Experimental Physics (ITEP), Moscow, Russia*
- ³² *Institute of Nuclear Physics, Moscow State University (SINP MSU), Moscow, Russia*
- ³³ *Institute for Nuclear Research of the Russian Academy of Sciences (INR RAN), Moscow, Russia*
- ³⁴ *Budker Institute of Nuclear Physics (SB RAS) and Novosibirsk State University, Novosibirsk, Russia*
- ³⁵ *Institute for High Energy Physics (IHEP), Protvino, Russia*
- ³⁶ *Universitat de Barcelona, Barcelona, Spain*
- ³⁷ *Universidad de Santiago de Compostela, Santiago de Compostela, Spain*
- ³⁸ *European Organization for Nuclear Research (CERN), Geneva, Switzerland*
- ³⁹ *Ecole Polytechnique Fédérale de Lausanne (EPFL), Lausanne, Switzerland*
- ⁴⁰ *Physik-Institut, Universität Zürich, Zürich, Switzerland*
- ⁴¹ *Nikhef National Institute for Subatomic Physics, Amsterdam, The Netherlands*
- ⁴² *Nikhef National Institute for Subatomic Physics and VU University Amsterdam, Amsterdam, The Netherlands*
- ⁴³ *NSC Kharkiv Institute of Physics and Technology (NSC KIPT), Kharkiv, Ukraine*
- ⁴⁴ *Institute for Nuclear Research of the National Academy of Sciences (KINR), Kyiv, Ukraine*
- ⁴⁵ *University of Birmingham, Birmingham, United Kingdom*
- ⁴⁶ *H.H. Wills Physics Laboratory, University of Bristol, Bristol, United Kingdom*
- ⁴⁷ *Cavendish Laboratory, University of Cambridge, Cambridge, United Kingdom*
- ⁴⁸ *Department of Physics, University of Warwick, Coventry, United Kingdom*
- ⁴⁹ *STFC Rutherford Appleton Laboratory, Didcot, United Kingdom*
- ⁵⁰ *School of Physics and Astronomy, University of Edinburgh, Edinburgh, United Kingdom*
- ⁵¹ *School of Physics and Astronomy, University of Glasgow, Glasgow, United Kingdom*
- ⁵² *Oliver Lodge Laboratory, University of Liverpool, Liverpool, United Kingdom*
- ⁵³ *Imperial College London, London, United Kingdom*
- ⁵⁴ *School of Physics and Astronomy, University of Manchester, Manchester, United Kingdom*
- ⁵⁵ *Department of Physics, University of Oxford, Oxford, United Kingdom*
- ⁵⁶ *Massachusetts Institute of Technology, Cambridge, MA, United States*
- ⁵⁷ *University of Cincinnati, Cincinnati, OH, United States*
- ⁵⁸ *University of Maryland, College Park, MD, United States*
- ⁵⁹ *Syracuse University, Syracuse, NY, United States*
- ⁶⁰ *Pontifícia Universidade Católica do Rio de Janeiro (PUC-Rio), Rio de Janeiro, Brazil, associated to ²*
- ⁶¹ *Institute of Particle Physics, Central China Normal University, Wuhan, Hubei, China, associated to ³*
- ⁶² *Departamento de Física, Universidad Nacional de Colombia, Bogota, Colombia, associated to ⁸*
- ⁶³ *Institut für Physik, Universität Rostock, Rostock, Germany, associated to ¹¹*
- ⁶⁴ *National Research Centre Kurchatov Institute, Moscow, Russia, associated to ³¹*
- ⁶⁵ *Yandex School of Data Analysis, Moscow, Russia, associated to ³¹*
- ⁶⁶ *Instituto de Física Corpuscular (IFIC), Universitat de Valencia-CSIC, Valencia, Spain, associated to ³⁶*
- ⁶⁷ *Van Swinderen Institute, University of Groningen, Groningen, The Netherlands, associated to ⁴¹*

^a *Universidade Federal do Triângulo Mineiro (UFMT), Uberaba-MG, Brazil*

^b *P.N. Lebedev Physical Institute, Russian Academy of Science (LPI RAS), Moscow, Russia*

^c *Università di Bari, Bari, Italy*

- ^d *Università di Bologna, Bologna, Italy*
^e *Università di Cagliari, Cagliari, Italy*
^f *Università di Ferrara, Ferrara, Italy*
^g *Università di Firenze, Firenze, Italy*
^h *Università di Urbino, Urbino, Italy*
ⁱ *Università di Modena e Reggio Emilia, Modena, Italy*
^j *Università di Genova, Genova, Italy*
^k *Università di Milano Bicocca, Milano, Italy*
^l *Università di Roma Tor Vergata, Roma, Italy*
^m *Università di Roma La Sapienza, Roma, Italy*
ⁿ *Università della Basilicata, Potenza, Italy*
^o *AGH - University of Science and Technology, Faculty of Computer Science, Electronics and Telecommunications, Kraków, Poland*
^p *LIFAELS, La Salle, Universitat Ramon Llull, Barcelona, Spain*
^q *Hanoi University of Science, Hanoi, Viet Nam*
^r *Università di Padova, Padova, Italy*
^s *Università di Pisa, Pisa, Italy*
^t *Scuola Normale Superiore, Pisa, Italy*
^u *Università degli Studi di Milano, Milano, Italy*
^v *Politecnico di Milano, Milano, Italy*